Redatuming of 2-D Wavefields Measured on an Arbitrary-Shaped Closed Aperture

Taskin, Ulaş; van der Neut, Joost; Gemmeke, Hartmut; van Dongen, Koen

DOI
10.1109/TUFFC.2019.2942453

Publication date
2020

Document Version
Accepted author manuscript

Published in
IEEE Transactions on Ultrasonics, Ferroelectrics and Frequency Control

Citation (APA)
Taskin, U., van der Neut, J., Gemmeke, H., & van Dongen, K. (2020). Redatuming of 2-D Wavefields Measured on an Arbitrary-Shaped Closed Aperture. *IEEE Transactions on Ultrasonics, Ferroelectrics and Frequency Control*, *67*(1), 173-179. Article 8844852. https://doi.org/10.1109/TUFFC.2019.2942453

Redatuming of 2-D Wavefields Measured on an Arbitrary-Shaped Closed Aperture

Ulas Taskin, Joost van der Neut, Hartmut Gemmeke, and Koen W. A. van Dongen

***Abstract*—Whole breast ultrasound scanning systems are used to screen a women's breast for suspicious lesions. Typically, the transducers are located at fixed positions at relatively large distances from the breast to avoid any contact with the breast. Unfortunately, these large distances give rise to large spatial domains to be imaged. These large domains hamper the applicability of imaging by inversion. To reduce the size of the spatial computational domain, we present a two-dimensional redatuming method based on Hankel decomposition of the measured field. With this method, the field measured over an arbitrary-shaped closed curve can be redatumed to a new curve enclosing a smaller spatial domain. Additional advantages of the proposed method are that it allows to account for the finite size and orientation of a transducer and that it is robust to noise. The proposed method is successfully validated using synthetic and measured data and the results show that the recorded field can be redatumed to any position in the embedding.**

***Index Terms*—redatuming, full-wave inversion, 2-D breast ultrasound.**

I. Introduction

ULTRASOUND is gaining interest as a modality for breast cancer detection. It has the advantage over conventional x-ray mammography that it has the capability to detect tumours in dense breasts and that it is a patient-friendly and safe imaging modality [1], [2]. Recent work on whole breast ultrasound focuses on water bath scanning systems [3], [4], [5]. As compared to hand-held systems, water bath scanning systems have the advantage that they are operator independent and need less scanning time. In addition, they provide transmission measurements together with reflection measurements by scanning the breast from all sides.

Recently, full-wave inversion methods are gaining attention as they have the potential to characterize the different tissues accurately using the reconstructed medium parameters [6], [7], [8]. These methods work especially well in case both reflection and through transmission measurements are available. However, full-wave inversion poses some challenges when applied in practice. First, full-wave inversion is computationally expensive. Several attempts have been made to overcome this problem, varying from source encoding [9] to the application of special accelerating and memory techniques [10].

To address the computational costs of full-wave inversion in geophysics, a method referred to as redatuming is commonly used [11], [12], [13], [14]. With this method the wave field is back-propagated from the plane where the measurements are made to a plane near the region of interest. In this way, a reduction of the computational domain and hence costs is achieved. The main approach in seismic is to redatum the measurement from one planar domain to another by using the Rayleigh II integral [15]. Since the measurement geometry is typically not planar for whole breast ultrasound, an alternative approach is needed. A continuation method is used for a similar problem faced with electromagnetic inversion for arbitrary surfaces [16].

In general, to extrapolate fields from a closed surface to another surface Green's second identity can be used. However, that requires the normal derivative of the pressure field along a closed surface. To overcome this problem the main approach is to find a Green's function that vanishes on the measurement surface [17], [18]. Since it is not easy to compute the required Green's function with Dirichlet boundary conditions, extrapolation from an arbitrary-shaped surface is not straightforward. Therefore, we use a different approach in this work. To account for an arbitrary shaped scanning setup, we propose Hankel function decomposition of the measured field to redatum the measurements to any location in the homogeneous background. The Hankel function is among the possible solutions of the two-dimensional (2-D) wave equation in cylindrical coordinates [19].

The organization of the paper is as follows. In section II, we start with a derivation of the theory behind the proposed redatuming method. Although the theory is derived for lossless media, it can be derived for a lossy media using the same approach. Next, we provide a method to account for the finite size of the receivers. In section III, we validate our method by showing results obtained with simulated data. In addition, we present reconstructions from real data before and after redatuming. In section IV, we discuss some details of the proposed method. Section V includes our concluding remarks.

II. Theory

Consider the 2-D scanning geometry depicted in Fig. 1. Here, the closed curves $\mathbb{S}$ and $\mathbb{S}'$ enclose the spatial domain $\mathbb{D}$. The curves $\mathbb{S}$ and $\mathbb{S}'$ are located in the homogeneous lossless embedding with constant speed of sound c. Contrasts in the acoustic medium parameters are only present in the spatial domain $\mathbb{D}$. A position in the spatial domain $\mathbb{R}^2$ is denoted in Cartesian coordinates by the vector (x, y) and in polar coordinates by the vector (r, ϕ), with $(x, y) = (r\cos(\phi), r\sin(\phi))$. Note that the origin lies inside $\mathbb{S}$ and $\mathbb{S}'$. All formulations are done in the temporal Fourier domain with angular frequency ω.

U. Taskin, J. van der Neut and K. W. A. van Dongen are with the Department of Imaging Physics, Delft University of Technology, Delft, the Netherlands.

H. Gemmeke is with KIT, Institute for Electronics and Data Processing, 76021 Karlsruhe, Germany.

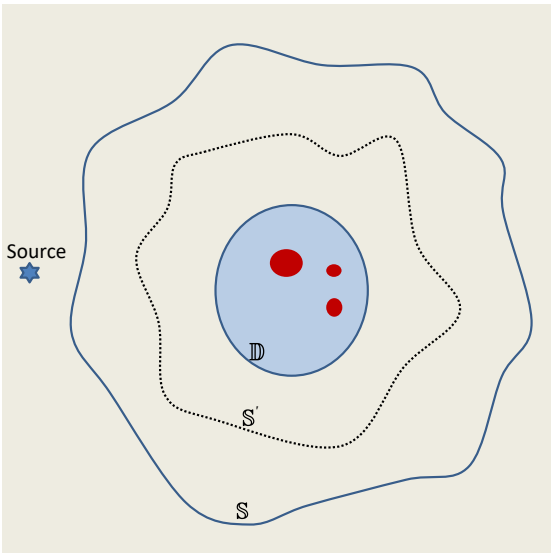

Fig. 1. Schematic representation of the setup. The source is located outside the receiver ring $\mathbb{S}$ enclosing our domain of interest $\mathbb{D}$. The measured wave field is redatumed from $\mathbb{S}$ to $\mathbb{S}'$.

A. Redatuming towards object of interest

The pressure field $p\left(r,\phi,\omega\right)$ measured in $\mathbb{S}$ satisfies the 2-D Helmholtz equation, which reads in polar coordinates

$$r^2\frac{\partial^2 p\left(r,\phi,\omega\right)}{\partial r^2}+r\frac{\partial p\left(r,\phi,\omega\right)}{\partial r}+\frac{\partial^2 p\left(r,\phi,\omega\right)}{\partial \phi^2} +r^2\frac{\omega^2}{c^2}p\left(r,\phi,\omega\right)=0. \tag{1}$$

This equation can be solved using the separation of variables method by separating the pressure field $p\left(r,\phi,\omega\right)$ in a radial and an angular part, hence

$$p\left(r,\phi,\omega\right)=\Gamma\left(r,\omega\right)\Phi\left(\phi\right). \tag{2}$$

Substituting equation (2) into (1) yields separate equations for $\Gamma\left(r,\omega\right)$ and $\Phi\left(\phi\right)$, namely

$$\frac{1}{\Gamma\left(r,\omega\right)}\left[r^2\frac{\partial^2\Gamma\left(r,\omega\right)}{\partial r^2}+r\frac{\partial\Gamma\left(r,\omega\right)}{\partial r}+r^2\frac{\omega^2}{c^2}\Gamma\left(r,\omega\right)\right] =\mu^2, \tag{3}$$

and

$$\frac{1}{\Phi\left(\phi\right)}\frac{\partial^2\Phi\left(\phi\right)}{\partial\phi^2}=-\mu^2, \tag{4}$$

with μ a constant. Equation (4) is a standard second-order differential equation whose solution equals

$$\Phi\left(\phi\right)=ae^{i\mu\phi}, \tag{5}$$

with arbitrary constant a and $-\pi<\phi\leq\pi$. To satisfy the boundary condition $\Phi\left(\pi\right)=\Phi\left(-\pi\right)$, μ needs to be an integer. This requirement limits the possible solutions for $\Phi(\phi)$ to

$$\Phi_n\left(\phi\right)=a_ne^{in\phi}, \tag{6}$$

with $n\in\mathbb{Z}$. Under this condition equation (3) becomes

$$r^2\frac{\partial^2\Gamma\left(r,\omega\right)}{\partial r^2}+r\frac{\partial\Gamma\left(r,\omega\right)}{\partial r}+\left(r^2\frac{\omega^2}{c^2}-n^2\right)\Gamma\left(r,\omega\right)=0. \tag{7}$$

Equation (7) is known as Bessel's differential equation and has as solution

$$\Gamma_n\left(r,\omega\right)=b_{n,1}(\omega)H_n^{(1)}\left(\frac{\omega}{c}r\right)+b_{n,2}(\omega)H_n^{(2)}\left(\frac{\omega}{c}r\right), \tag{8}$$

where the Hankel functions $H_n^{(1)}\left(\frac{\omega}{c}r\right)$ and $H_n^{(2)}\left(\frac{\omega}{c}r\right)$ represent outward and inward propagating cylindrical waves, respectively. By placing the origin of our coordinate system inside $\mathbb{S}$ and $\mathbb{S}'$ we know that the scattered field is only described by outward propagating waves. Consequently, all coefficients $b_{n,2}(\omega)$ are equal to zero. By combining equations (2), (6), (8) and the condition $b_{n,2}(\omega)=0$, the solutions of equation (1) for each n are, up to a constant, equal to

$$p_n\left(r,\phi,\omega\right)=\Gamma_n\left(r,\omega\right)\Phi_n\left(\phi\right)=H_n^{(1)}\left(\frac{\omega}{c}r\right)e^{in\phi}. \tag{9}$$

The final solution is obtained by taking a linear combination of the solutions given in (9), hence

$$p\left(r,\phi,\omega\right)=\sum_{n=-N}^{N}c_n(\omega)H_n^{(1)}\left(\frac{\omega}{c}r\right)e^{in\phi}. \tag{10}$$

To find the complex valued coefficients $c_n(\omega)$ of equation (10), the pressure field $p(r,\phi,\omega)$ is matched to the M measurements $d_m(\omega)$, where $d_m(\omega)$ is the field measured by the m^{th} receiver located on $\mathbb{S}$. Consequently, the unknown coefficients $c_n(\omega)$ are obtained by solving the following system of equations

$$\sum_{n=-N}^{N}c_n(\omega)H_n^{(1)}\left(\frac{\omega}{c}r_m\right)e^{in\phi_m}=d_m\left(\omega\right), \tag{11}$$

for all m. Rewriting equation (11) in matrix-vector notation gives

$$\begin{bmatrix} H_{-N}^{(1)}\left(\frac{\omega}{c}r_1\right)e^{-iN\phi_1} & \cdots & H_{N}^{(1)}\left(\frac{\omega}{c}r_1\right)e^{iN\phi_1}\\ \vdots & \ddots & \vdots\\ H_{-N}^{(1)}\left(\frac{\omega}{c}r_M\right)e^{-iN\phi_M} & \cdots & H_{N}^{(1)}\left(\frac{\omega}{c}r_M\right)e^{iN\phi_M}\end{bmatrix} \times\begin{bmatrix}c_{-N}(\omega)\\ \vdots\\ c_N(\omega)\end{bmatrix}=\begin{bmatrix}d_1(\omega)\\ \vdots\\ d_M(\omega)\end{bmatrix} \tag{12}$$

or, in shorthand notation,

$$\underline{\underline{Q}}\,\underline{c}=\underline{d}, \tag{13}$$

with $\underline{\underline{Q}}$ a $(M)\times(2N+1)$ matrix with elements $Q_{m,n}=H_n^{(1)}\left(\frac{\omega}{c}r_m\right)e^{in\phi_m}$, $\underline{c}$ a vector of length $(2N+1)$ with elements $c_n(\omega)$, and $\underline{d}$ a vector of length M with elements $d_m(\omega)$. For the convergence, sufficient number of data points (M) need to be provided for the $(2N+1)$ coefficients for the Hankel functions. In this work, we use Tikhonov regularization to find the coefficients $c_n(\omega)$, consequently

$$\underline{c}=(\underline{\underline{Q}}^{\dagger}\,\underline{\underline{Q}}+\alpha I)^{-1}\underline{\underline{Q}}^{\dagger}\underline{d}, \tag{14}$$

where I is a unit matrix, α is a regularization parameter, and $\underline{\underline{Q}}^{\dagger}$ denotes the adjoint of $\underline{\underline{Q}}$.

Once the coefficients $c_n(\omega)$ are found, the field can be computed at any location outside $\mathbb{D}$ using equation (10). In

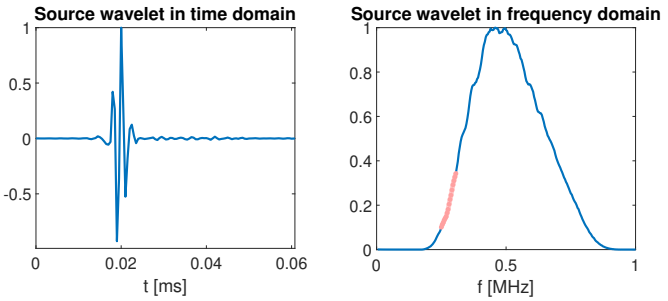

Fig. 2. Normalized source excitation profile in time (left) and frequency (right) domain. The red dots show the frequency range used for inversion.

this way, we can redatum the wave field measured at $\mathbb{S}$ to the domain $\mathbb{S}'$. Although redatuming is explained for the receiver side using the outward propagating field, it is also possible to apply the same procedure for the source side by using the inward propagating field. Finally, for an accurate reconstruction of the wave field it is important to satisfy the sampling criterion as this defines the number of coefficients needed to describe the wave field [20].

B. Application of finite-sized receiver

For the receiver it is important to account for its size and orientation. The field measured with a finite-sized receiver of aperture length L, can be written as an integral over its active curve of length $2r_m\theta$. It is assumed here that, the receiver ring $\mathbb{S}$ is a circle centered at the origin. Consequently, for transducers oriented towards the origin the measurement $d_m(\omega)$ equals

$$d_m(\omega) = d(r_m, \phi_m, \omega) = \int_{-\theta}^{+\theta} p(r_m, \phi_m + \phi^{'}) d\phi^{'}. \quad (15)$$

When we combine equations (10) and (15) and alter the order of integration, it follows that

$$d_m(\omega) = \sum_{n=-N}^{N} c_n(\omega) T_n H_n^{(1)} \left(\frac{\omega}{c} r_m\right) e^{in\phi_m}, \quad (16)$$

where the finite size of the transducer is accounted for via the constant T_n

$$T_n = \int_{-\theta}^{+\theta} e^{in\phi^{'}} d\phi'. \quad (17)$$

III. Results

The proposed method is tested on synthetic and experimental data. To show its practical applicability, we present an example where we apply contrast source inversion (CSI) [21] on measured data before and after redatuming.

A. Synthetic example

1) Configuration: A full-wave method based on a frequency-domain integral equation formulation is used to solve the forward problem [22], [23]. A source is located outside $\mathbb{S}$ at $(x_s, y_s) = (0.248\ \mathrm{m}, 0.035\ \mathrm{m})$ and generates a Gaussian modulated pressure field with 0.5 MHz central frequency. The source's excitation profile is shown in Fig. 2. In total 450 receivers are used to measure the scattered field. The time span of the simulation is set to 268 µs with a step size $\Delta t = 0.5$ µs. The spatial domain equals $0.1\ \mathrm{m} \times 0.1\ \mathrm{m}$ and is discretized with a uniform grid size $\Delta x = 0.5$ mm. The grid size corresponds to six points per wavelength at central frequency. A rectangular object ($0.02\ \mathrm{m} \times 0.05\ \mathrm{m}$) is placed at the center. The speed of sound of the background medium is 1490 m/s and of the object 1547 m/s. The background medium and the object have the same mass density $\rho = 1000\ \mathrm{kg/m^3}$ and are both lossless.

2) Synthetic Results: First, we consider the case where the field measured with a circular array is redatumed, see Fig. 3. For this purpose, the simulated pressure field is measured at $r = 0.09$ m using 450 point receivers and reconstructed using Hankel functions, see Fig. 3 first row. Then, the measured field at $r = 0.09$ m (blue circle) is redatumed to $r = 0.05$ m (red circle). The redatumed and modelled fields at the red circle are shown in Fig. 3 second row. The amplitudes of both fields are normalized by the same constant. These single frequency results clearly show that both the amplitude and the phase of the fields match each other perfectly. Finally, the performance of the proposed method is tested using an arbitrary shaped scanning setup. The third row of Fig. 3 shows the results for redatuming from one arbitrary surface to another. These results agree with the observation that the proposed method does not depend on the applied configuration, as long as the field is measured along a closed curve. Note that, we used $M = 450$ number of data points and $2N+1 = 211$ coefficients for these experiments.

To examine the similarities between the measured and reconstructed wavefield for all frequency components, time domain results are shown in Fig. 4 and 5. Fig. 4 shows the measurements at five receiver locations at the transmission side; Fig. 5 at the reflection side. Note that all fields are normalized using the same constant.

Second, to examine the robustness of the proposed method, the results of a noisy experiment is shown in Fig. 6. White noise with an amplitude equal to 7.5% of the maximum amplitude of the recorded data set is added to the measured signal. A noise-free measurement is plotted together with a noisy measurement in the second graph and with reconstructed field form the noisy measurement in the third graph in Fig. 6. For the noisy measurement, the signal to noise ratio (SNR) equals 7.1 dB. The reconstructed field from this noisy measurement has an SNR = 10.3 dB. It is concluded from both these values and the results shown in Fig. 6 that with the proposed method the noise in the measurement is slightly suppressed. This is due to the fact that projecting the measurement on the Hankel functions filters out some noise. Careful analysis of denoising by Hankel decomposition is beyond the scope of this work but initial results show some potential. To exploit this aspect further, one can apply inversion using an l_1-solver [24].

Finally, accounting for a finite-sized receiver is investigated. In particular, we test for receivers with an active aperture of length $L = \lambda, 2\lambda,$ and 4λ. The pressure fields measured with these finite-sized receivers at $r = 0.09$ m are given in Fig. 7 together with the reconstructed fields. Reconstructed and measured fields are matching each other perfectly when the

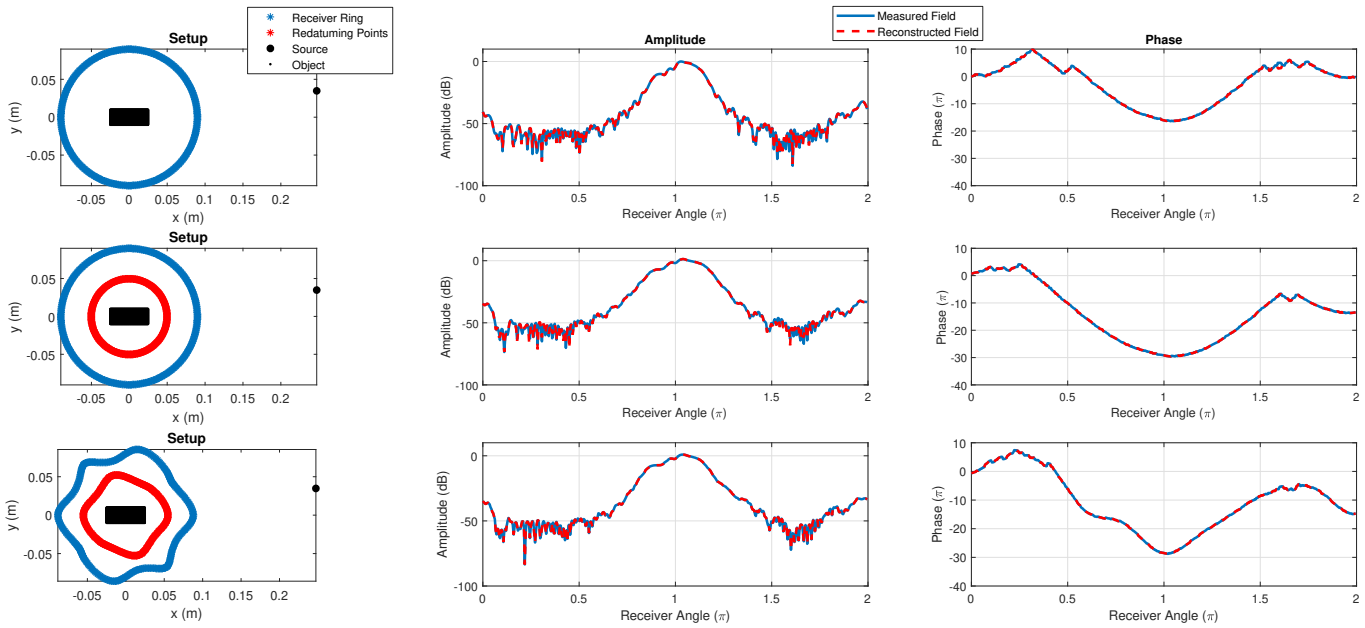

Fig. 3. Single frequency (0.5 MHz) results using point receivers. The setups are given in the first column. The first row shows the synthetically measured and reconstructed pressure fields at the blue surface. The second and third rows show the synthetically measured and redatumed pressure field at the red surface. The redatumed field is computed from the measurements at the blue surface.

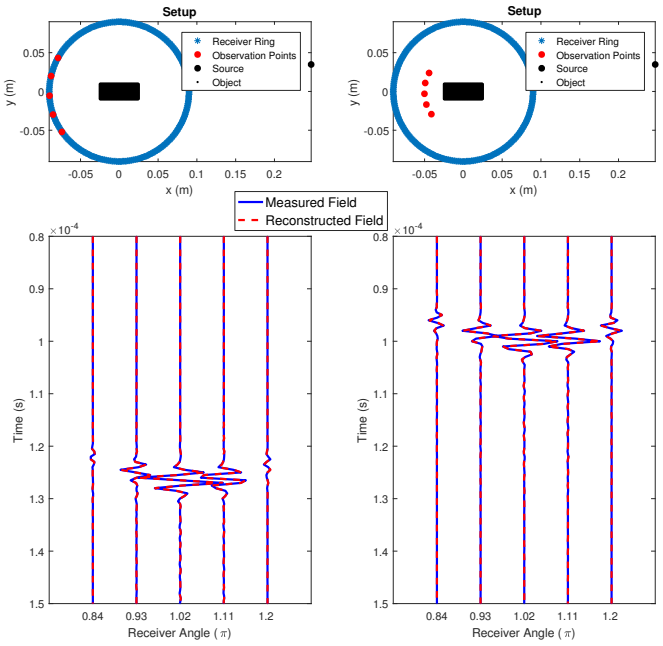

Fig. 4. Time domain results for transmission measurements using point receivers. The setup is shown in the first row; the source (black dot) is on the right of the original receiver array (blue dots) and the redatumed locations (red dots). A-scans of the measured (blue) and reconstructed (red) wave fields are shown in the second row; (left) with the redatumed locations coinciding the original receiver locations and (right) positioned inside the receiver ring.

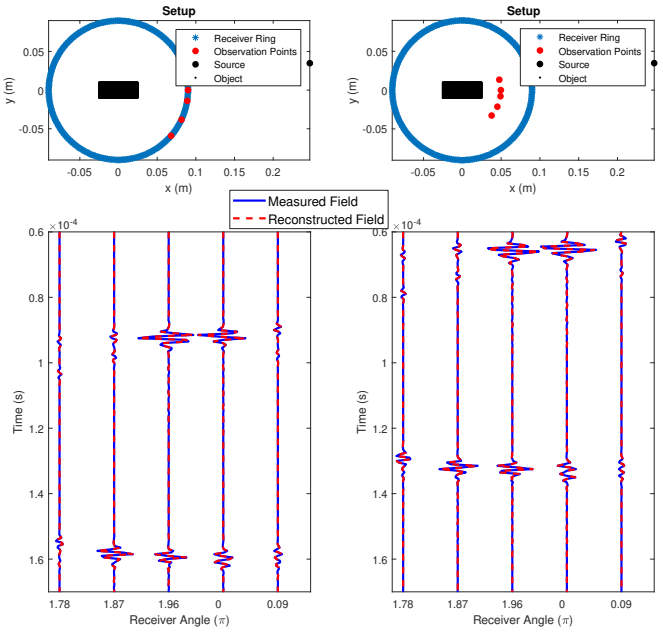

Fig. 5. Same as Fig. 4, but now for reflection measurements.

signal is above -40 dB. Differences in phase and amplitude occur when the amplitude of the signal is below -40 dB. This is due to the fact that the same fixed number of coefficients $c_n(\omega)$ are used to reconstruct the fields. The areas where the signal amplitude is above -40 dB are highlighted with a red square.

B. Experimental example

1) Configuration: The Delft Breast Ultrasound Scanner (DBUS) is used to validate our method using measured data [25]. This system has a configuration similar to the one used for the synthetic examples. A source located at a $r = 0.25$ m operates at 0.5 MHz central frequency. The circular receiver array has a radius of 0.1 m. A complete measurement covers 45 source and 450 receiver locations. The object is a rectangular agar phantom containing two copper threads and one plastic straw. A sketch of the system together

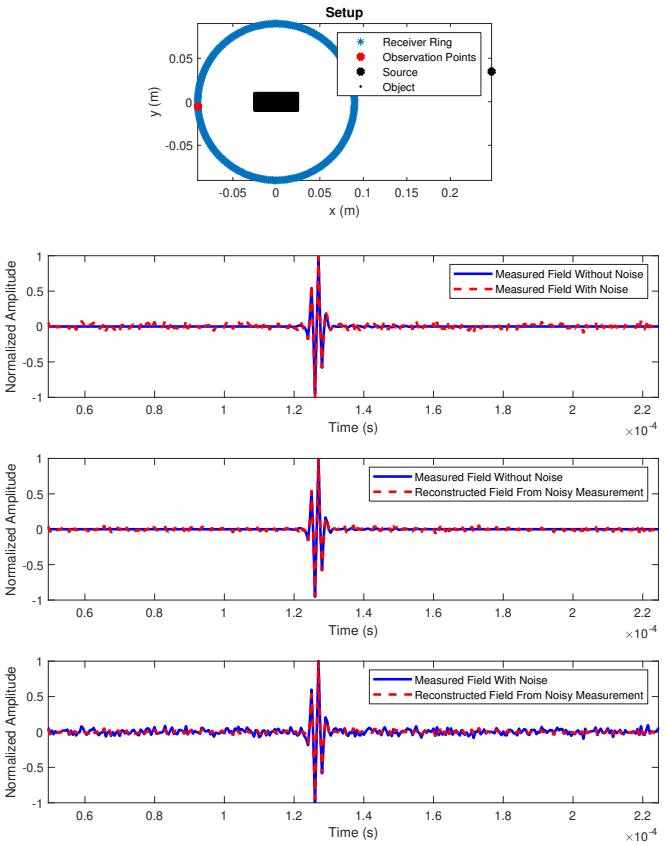

Fig. 6. Time domain results showing the robustness of the method to noise. Setup is given at the first row. The second row shows noisy and noise-free measurements. The third row shows the noise free measurement and reconstructed signal from a noisy measurement. The fourth row shows the noisy measurement and reconstructed signal from a noisy measurement.

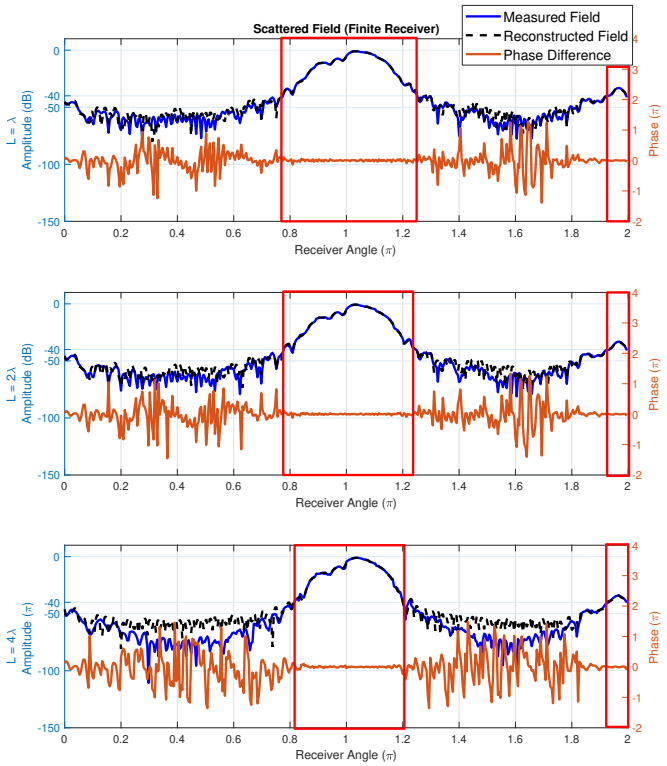

Fig. 7. Single frequency (0.5 MHz) results using finite-sized receivers. The measured and reconstructed pressure fields using a receiver of length $L = \lambda, 2\lambda,$ and4λ (top to bottom). The receivers are located at the $r = 0.09$ m circle with the normal oriented to the center. Red squares enclose the signal when the amplitude is above -40 dB.

with a reconstruction of the phantom using Synthetic Aperture Focusing Technique (SAFT) [26] is shown in Fig. 8.

2) Experimental results: Contrast source inversion (CSI) is applied to the data from the DBUS system [6], [21], [27]. Five frequency components between 0.25 MHz and 0.3 MHz are used for the inversion. Reconstruction result after 128 iterations without applying redatuming is shown in the first row of Fig. 9. The second row shows the result after redatuming the data to the circular receiver array with radius $r = 0.05$ m. The results are highly similar. The small variations visible are mainly caused by the misfit between the actual locations of the receivers and the grid points in the computational domain. With the help of redatuming, it is possible to let the receiver locations coincide exactly with the grid points of the computational domain. After redatuming, the resulting spatial domain has become four times smaller; only 204×204 pixels out of the original 406×406 pixels are preserved.

Reducing the size of the spatial domain allows us to increase the number of frequency components for the inversion without affecting the total computational load. The gain in performance is clearly visible in the third row of Fig. 9, where we increase the number of frequency components from 5 to 20. The computation time for this latter case is the same as for the original case using four components only (neglecting the time spent on redatuming).

IV. Discussion

The method proposed in this work to redatum the measured fields is computationally efficient and suitable for water bath scanners that have a closed acquisition surface. Typically, those systems have a measurement radius greater than 20 cm. Hence, redatuming the measurements closer to the breast that may have an effective diameter of 12 cm [28] can reduce the computation time for inversion. The proposed method may also be useful for a setup that has a smaller radius. For the latter case, a non-perfect spherical or circular acquisition boundary can be easily mapped on a Cartesian grid. This is beneficial for integral-type inversion methods where FFT's may be used to compute the convolutions with the Green's function efficiently.

In this work, we use contrast source inversion (CSI) algorithm to solve the scattering integral equation iteratively. To compute the spatial convolutions with the Green's function efficiently we use FFT's. This requires the receivers and unknowns to be located inside the same spatial computation domain. Regarding the presented example in the experimental results section, the computation time for each iteration decreased approximately by a factor four. In addition, after redatuming the wave field to a smaller domain, CSI converges faster compared to the normal case using the same five frequency components, see Fig. 10. These results show that

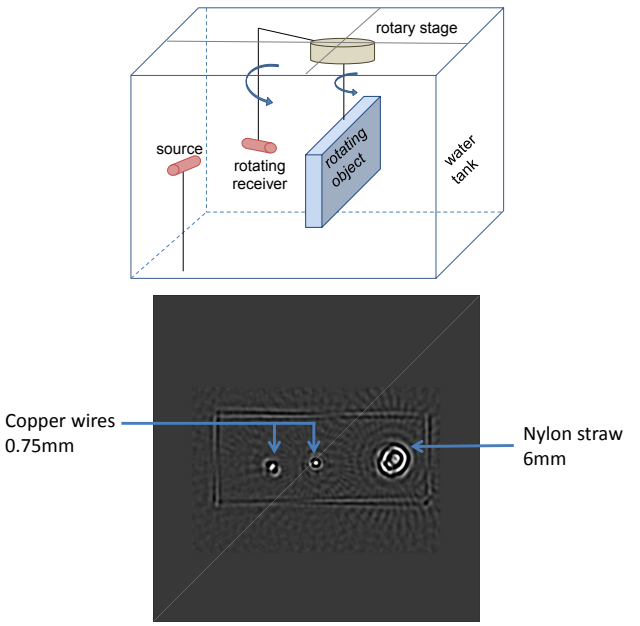

Fig. 8. Sketch of the DBUS system (top). Reconstruction of the phantom using SAFT (bottom).

CSI has a supralinear cost functional and that the total computational gain is higher than a factor four in this case. Similar observations have been reported for the forward problem in the past [29]. There it was shown that reducing the domain of interest hides the influence of the unknowns located at points of zero contrast from the minimization procedure, thereby improving the condition number of the system and thus the convergence rate.

In a real experiment, some problems can occur with the scanning setup such as undersampled measurements, errors in receiver locations, etc. Since these problems affect any inversion algorithm, here it is assumed that they are already taken care of beforehand. In fact, we showed in the experimental results that the proposed method works for measured data.

The redatuming method presented in this work is computationally very efficient. For example, generating the single frequency results shown in Fig. 3. takes less than a second. On the other hand, each iteration of CSI takes around 5.1 minutes before redatuming and around 1.3 minutes after redatuming (using the same five frequency components). For each data set, redatuming has to be done only once while CSI has to be iterated many times. Note that, all computations are done on a Windows server with a Windows Server 2008 R2 Enterprise 64-bit operating system and Intel Xeon E5620 CPU (2.4 GHz). Redatuming is applied in MATLAB R2016b and CSI is running in a FORTRAN90 environment accelerated with OMP routines.

V. Conclusion

With redatuming, the measured acoustic wave field is transformed into a data set that is representative for a recording of the same wave field but now at a different location. A common way to migrate the wave field from one surface to another is by employing Kirchhoff integrals. Unfortunately, redatuming methods based on Kirchhoff migration fail for breast ultrasound where the recording surface is often curved and only the pressure field is measured.

To overcome these problems, we developed a novel redatuming method where the measured pressure field is described as a series of Hankel functions to account for the radii of the receiver locations, complex exponentials to account for angular variations and corresponding complex coefficients as weighting factors. The resulting linear system of equations is solved using Tikhonov regularization. Once the coefficients are found, the field can be redatumed to any location in the

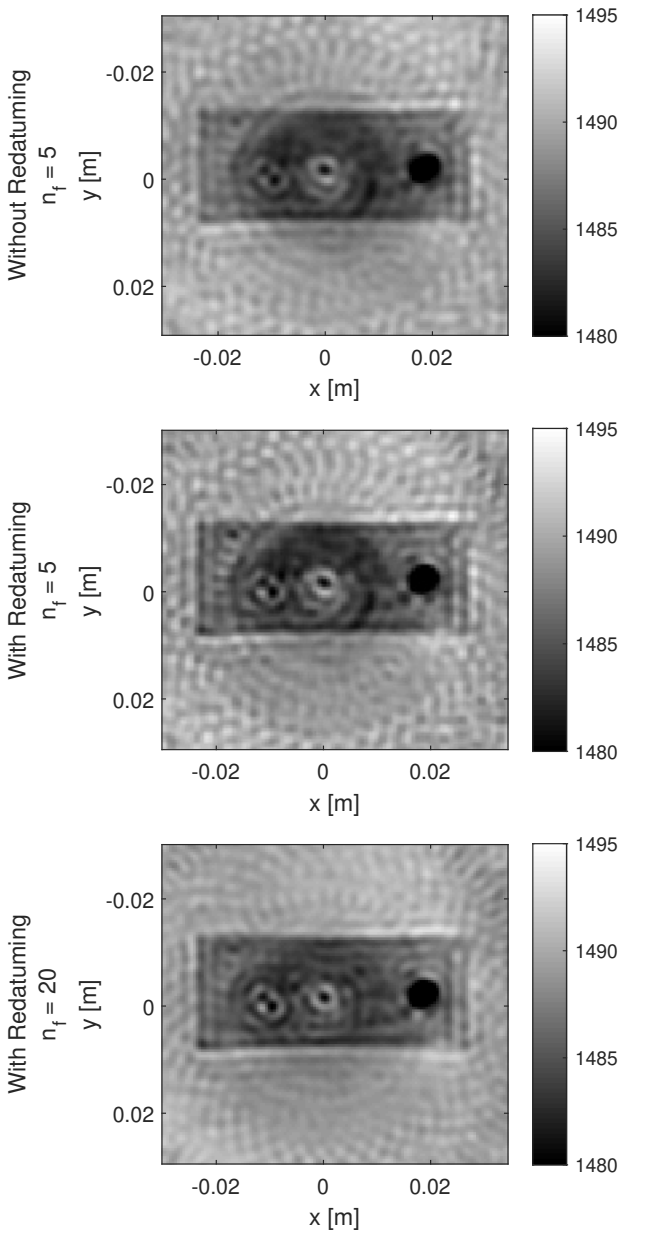

Fig. 9. Results obtained with CSI after 128 iterations with and without redatuming. The top image shows the reconstruction using five frequency components without redatuming, the middle the reconstruction after the same five frequency components with redatuming, and the bottom the reconstruction using 20 frequency components after redatuming. The gray scale indicates speed of sound values in $\mathrm{m/s}$.

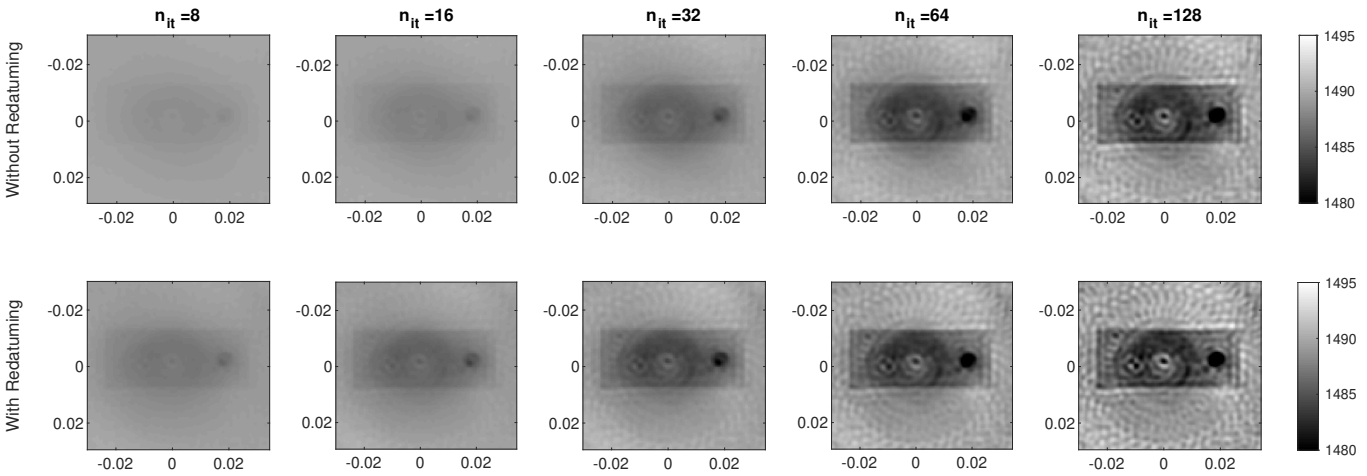

Fig. 10. CSI results before and after redatuming for an increasing number of iterations ($n_{it} = 8, 16, 32, 64,$ and 128). Note that these results are obtained using the same five frequency components. The gray scale indicates speed of sound values in $\mathrm{m/s}$.

homogeneous embedding.

Results based on measured data show that redatuming to any location in the homogeneous embedding is possible and that it indeed leads to a reduction in computational costs. In addition, it is shown using synthetic data that it is possible to redatum when the actual measurements are done using finite-sized receivers. Finally, with a synthetic example, it is shown that the proposed method itself is robust against random noise and it also has the potential to act as a denoiser.

ACKNOWLEDGMENT

We would like to thank Lars Heijnsdijk, Leo Hoogerbrugge, and Peter M. van den Berg for their contributions for developing the ideas presented in this work.

REFERENCES

[1] P. B. Gordon and S. L. Goldenberg, "Malignant breast masses detected only by ultrasound. A retrospective review," *Cancer*, vol. 76, no. 4, pp. 626–630, 1995.

[2] N. Duric, P. Littrup, L. Poulo, A. Babkin, R. Pevzner, E. Holsapple, O. Rama, and C. Glide, "Detection of breast cancer with ultrasound tomography: First results with the computed ultrasound risk evaluation (cure) prototype," *Medical physics*, vol. 34, no. 2, pp. 773–785, 2007.

[3] N. Duric, P. Littrup, S. Schmidt, C. Li, O. Roy, L. Bey-Knight, R. Janer, D. Kunz, X. Chen, J. Goll *et al.*, "Breast imaging with the softvue imaging system: First results," in *Medical Imaging 2013: Ultrasonic Imaging, Tomography, and Therapy*, vol. 8675. International Society for Optics and Photonics, 2013, p. 86750K.

[4] J. Wiskin, D. Borup, S. Johnson, M. Andre, J. Greenleaf, Y. Parisky, and J. Klock, "Three-dimensional nonlinear inverse scattering: Quantitative transmission algorithms, refraction corrected reflection, scanner design and clinical results," in *Proceedings of Meetings on Acoustics ICA2013*, vol. 19, no. 1. ASA, 2013, p. 075001.

[5] N. Ruiter, M. Zapf, R. Dapp, T. Hopp, W. Kaiser, and H. Gemmeke, "First results of a clinical study with 3D ultrasound computer tomography," in *Ultrasonics Symposium (IUS), 2013 IEEE International*. IEEE, 2013, pp. 651–654.

[6] N. Ozmen, R. Dapp, M. Zapf, H. Gemmeke, N. V. Ruiter, and K. W. A. van Dongen, "Comparing different ultrasound imaging methods for breast cancer detection," *IEEE Trans. Ultrason., Ferroelectr, Freq. Control*, vol. 62, no. 4, pp. 637–646, 2015.

[7] M. Pérez-Liva, J. Herraiz, J. Udías, E. Miller, B. Cox, and B. Treeby, "Time domain reconstruction of sound speed and attenuation in ultrasound computed tomography using full wave inversion," *The Journal of the Acoustical Society of America*, vol. 141, no. 3, pp. 1595–1604, 2017.

[8] G. Y. S. Sandhu, C. Li, O. Roy, S. Schmidt, and N. Duric, "High-resolution quantitative whole-breast ultrasound: in vivo application using frequency-domain waveform tomography," in *Medical Imaging 2015: Ultrasonic Imaging and Tomography*, vol. 9419. International Society for Optics and Photonics, 2015, p. 94190D.

[9] K. Wang, T. Matthews, F. Anis, C. Li, N. Duric, and M. A. Anastasio, "Waveform inversion with source encoding for breast sound speed reconstruction in ultrasound computed tomography," *IEEE transactions on ultrasonics, ferroelectrics, and frequency control*, vol. 62, no. 3, pp. 475–493, 2015.

[10] P. Mojabi and J. LoVetri, "Ultrasound tomography for simultaneous reconstruction of acoustic density, attenuation, and compressibility profiles," *The Journal of the Acoustical Society of America*, vol. 137, no. 4, pp. 1813–1825, 2015.

[11] J. R. Berryhill, "Wave-equation datuming before stack," *Geophysics*, vol. 49, no. 11, pp. 2064–2066, 1984.

[12] S. Tegtmeier-Last, A. Gisolf, and D. Verschuur, "A data-mapping approach to 3-D wavefield redatuming," *Geophysical Journal International*, vol. 172, no. 2, pp. 759–769, 2008.

[13] G. Schuster and M. Zhou, "A theoretical overview of model-based and correlation-based redatuming methods: Geophysics, 71," *SI103–SI110*, 2006.

[14] P. Haffinger, A. Gisolf, and P. M. Van Den Berg, "Towards high resolution quantitative subsurface models by full waveform inversion," *Geophysical Journal International*, vol. 193, no. 2, pp. 788–797, 2013.

[15] D. Gisolf and E. Vershuur, *The principles of quantitative acoustical imaging*. EAGE Publications bv, 2010.

[16] Ö. Ozdemir and H. Haddar, "Preprocessing the reciprocity gap sampling method in buried-object imaging experiments," *IEEE Geoscience and Remote Sensing Letters*, vol. 7, no. 4, pp. 756–760, 2010.

[17] S. A. Johnson, Y. Zhou, M. Tracy, M. J. Berggren, and F. Stenger, "Inverse scattering solutions by a sinc basis, multiple source, moment method—part iii: Fast algorithms," *Ultrasonic Imaging*, vol. 6, no. 1, pp. 103–116, 1984.

[18] A. C. Ramírez and A. B. Weglein, "Green's theorem as a comprehensive framework for data reconstruction, regularization, wavefield separation, seismic interferometry, and wavelet estimation: A tutorial," *Geophysics*, vol. 74, no. 6, pp. W35–W62, 2009.

[19] F. B. Jensen, W. A. Kuperman, M. B. Porter, and H. Schmidt, *Computational ocean acoustics*. Springer Science & Business Media, 2011.

[20] F. Simonetti, L. Huang, and N. Duric, "On the spatial sampling of wave fields with circular ring apertures," *Journal of Applied Physics*, vol. 101, no. 8, p. 083103, 2007.

[21] P. M. van den Berg and A. Abubakar, "Contrast source inversion method: State of art," *Progress in Electromagnetic Research*, vol. 34, no. -, pp. 189–218, 2001.

[22] U. Taskin, N. Ozmen, H. Gemmeke, and K. W. A. van Dongen, "Modeling breast ultrasound; on the applicability of commonly made approximations," *Archives of Acoustics*, vol. 43, no. 3, 2018.

[23] M. D. Verweij, B. E. Treeby, K. W. A. Dongen, and L. Demi, "Simulation of ultrasound fields," in *Comprehensive Biomedical Physics*,

A. Brahme, Ed. Oxford: Elsevier Science B.V., 2014, ch. 2.19, pp. 465–500.

[24] J. van der Neut and F. J. Herrmann, "Interferometric redatuming by sparse inversion," *Geophysical Journal International*, vol. 192, no. 2, pp. 666–670, 2012.

[25] L. Heijnsdijk, E. Jansen, U. Taskin, H. den Bok, E. Bergsma, E. Noothout, N. de Jong, and K. W. A. van Dongen, "First steps towards the Delft Breast Ultrasound Scanning system (DBUS)," *Int. Workshop on Medical Ultrasound Tomography*, pp. 131–136, 2017.

[26] V. Schmitz, S. Chakhlov, and W. Müller, "Experiences with synthetic aperture focusing technique in the field," *Ultrasonics*, vol. 38, no. 1-8, pp. 731–738, 2000.

[27] A. B. Ramirez and K. W. A. van Dongen, "Sparsity constrained contrast source inversion," *The Journal of the Acoustical Society of America*, vol. 140, no. 3, pp. 1749–1757, 2016.

[28] S.-Y. Huang, J. M. Boone, K. Yang, N. J. Packard, S. E. McKenney, N. D. Prionas, K. K. Lindfors, and M. J. Yaffe, "The characterization of breast anatomical metrics using dedicated breast CT," *Medical physics*, vol. 38, no. 4, pp. 2180–2191, 2011.

[29] K. W. A. van Dongen, C. Brennan, and W. M. Wright, "Reduced forward operator for electromagnetic wave scattering problems," *IET Science, Measurement & Technology*, vol. 1, no. 1, pp. 57–62, 2007.